CORRECTING SAR FORESHORTENING ERROR WITH A DIGITAL ELEVATION MODEL

D. S. Oliver
Utah State University
Logan, Utah

Abstract

Synthetic Aperture Radar imagery of high relief areas suffers from terrain induced distortion known as foreshortening. This distortion prevents accurate registration to images from other sources, such as Landsat TM images. If a Digital Elevation Model is used to provide accurate elevation estimates during the SAR image formation processing, foreshortening can be eliminated. However, because of processing complexity, this operation this is not typically done. This paper shows how the end user of SAR imagery can use a Digital Elevation Model and platform ephemeris to estimate the foreshortening error and correct the imagery. Results of an actual SIR-C SAR and Landsat TM image coregistration shows an improvement in cross track registration error from 9.17 pixels to 1.17 pixels when this method is applied.

Introduction

A. Earth Remote Sensing

Earth remote sensing is the science of using images of the earth from space borne or airborne instruments to get information about the ground. These images are used for many purposes, including vegetation mapping, geologic mapping, and urban planning. Geographers make use of these images to create accurate and detailed maps of surface features such as land use or ground cover.

One of the best sources for these images in optical and near IR wavelengths is from the Landsat satellites. Data from the thematic mapper(TM) instrument on the landsat satellites has been available since 1982 with the launch of Landsat-4. Lower resolution data from the multispectal scanner instrument (MSS) has been available since 1972 when Landsat-1 was launched.

In addition to optical Landsat images, SAR radar images are now available. Several countries have launched satellites containing SAR radar mapping instruments. These include Japan's JERS-1 launched in 1992, the European Space Agency's ERS-1 and ERS-2, launched in 1991 and 1996, respectively, Canada's Radarsat, launched in 1995, and the United States' Shuttle Imaging Radar experiments, which have been flown on the Space Shuttle in 1982, 1985, and 1994. NASA has an airborne SAR instrument, the AIRSAR, which has been in use since 1988, and the US briefly had a satellite SAR instrument available on Seasat in 1978.

A radar instrument has several advantages over a visible sensor. Since it does not rely on the sun for illumination of the target, it can operate in both dark and sunlit regions. Ground features are not obscured by clouds, fog, or haze in the atmosphere. SAR backscatter is sensitive to surface roughness as well as ground cover material. Also, for a few special surface materials such as very dry sand, the radar penetrates below the surface of the ground. These features make it a good complement to the typical visible light sensors.

B. Combined SAR/Landsat studies

There is significant interest among the remote sensing community in using images from these new synthetic aperture radar sources in conjunction with optical images. In a unified data set, both the surface reflectance in the optical to infrared wavelength region and the radar backscatter is known for each point on the ground. This combined data set can used for several purposes. Landsat and ERS-1 SAR data have been combined for forestry mapping [2]. Landsat and airborne SAR data have been combined for forest monitoring [10], vegetation mapping [12] and the study of ice sheets [8]. Seasat SAR imagery has also been combined with Landsat for geologic mapping [7], and ice sheet study [9]. Landsat and SIR-A data have been combined for the study of African desert areas for groundwater exploration [13] and locating villages [14].

C. Registration Error

The major obstacle in creating a Landsat-SAR unified data set is distortion of the SAR image. The primary cause of distortion is elevation changes on the ground over the area that is being imaged, known as foreshortening, layover, and shadow [5]. A cross track shift in pixel location related to its elevation is the net result of this distortion. It causes a control-point-matching based image registration process to have a large registration error. This registration error is typically on the order of ten pixels in the cross track direction. Without this distortion in the image, registration accuracies on the order of one pixel error are possible. One approach to overcoming the registration difficulty is to use a Digital Elevation

Model to find the size of the distortion, and to use this information to resample the SAR image to have much less distortion

A 1979 NASA study [17] on registration of SAR imagery to Landsat images concluded that "investigations should continue to determine the differences involved in registering satellite SAR images with corrected Landsat MSS images, and techniques for modeling these geometric distortions should be investigated"

Since that time, several solutions have been proposed. In 1983 Naraghi et al.[3] proposed a rectification model which uses a DEM to create a simulated SAR image. The actual SAR image is registered to the simulated SAR image using a large number of control points. Next, in 1987 Kwok et al. [4] proposed a method more similar to the one developed in this study. A DEM was used as a supplementary data set during the SAR image formation process, and a correction is made to the slant range to compensate for foreshortening.

However, because DEM information is not always available and because performing the correction dramatically increases the computation time for image formation, this procedure is not typically implemented in SAR image formation processing. None of the actual studies mentioned above used a DEM foreshortening correction procedure. Each one used a ground control point (GCP) based image registration based on the raw SAR images. Most [8,10,14] did not mention the quality of the resulting registration. Several of the studies [2,9,12] concluded that pixel-by-pixel comparison of the SAR to Landsat data was not useful because terrain variations prevented an adequate registration. One of these [9] reported a 10 pixel error directly using ground control points to register TM and SAR, which is the same amount of error found in this study before foreshortening corrections.

D. Proposed Solution

There seems to be a gap between the theory of correcting SAR distortion using a DEM and its use in practical applications. This research focused on developing a method for creating a geometrically corrected SAR data set which can be applied by the end user, who has access only to the final SAR image and platform ephemeris information. An algorithm for applying the elevation model to correct the foreshortening distortion will be presented, as well as the results obtained by applying this algorithm to registering an actual SIR-C SAR image to a Landsat TM image in an area of high terrain variation.

Landsat and SAR Image Characteristics

A. Landsat image characteristics

The source of optical images used in this study is the Thematic Mapper(TM) instrument on a Landsat satellite. The TM sensor records data in seven different spectral bands [16]. Bands 1,2, and 3 are visible wavelength bands in blue, green, and red, respectively. Bands 4,5, and 7 are near infrared bands. Band 6 is in the mid infrared, or thermal region. The landsat image used in this study was recorded on September 25, 1994 in landsat path number 38, row number 31, and was purchased directly from Eosat. This area is over the Northeast corner of Utah.

The TM sensor looks straight down, or from a nadir view. Because of this, the Landsat images have little geometric distortions from viewing angle complexities. Each pixel in the landsat image is an eight bit digital number which represents the intensity of light received at the sensor in that part of the spectrum. Each pixel covers a 30-by-30 meter square on the ground, except for band 6, which covers a 120-by-120 meter square. The total image size for the image in the study is 6967-by-5965 pixels. In order to facilitate more rapid processing, a smaller area of interest was extracted, with dimension 1371-by-1711 pixels.

B. SAR image characteristics

The second set of images in this study is from SIR-C, which is the third Shuttle Imaging Radar experiment. This was a radar instrument flown on two flights on the space shuttle Endeavour: first in April 1994 on mission STS-59, and again in September and October 1994. The purpose of the mission, according to NASA, was to collect data needed to study ecosystems, climatic and geological processes, the hydrologic cycle, and ocean circulation [6]. It was also designed as a precursor to a radar earth observing instrument on a free flying satellite planned for the future. The SAR image in this study was recorded on October 2, 1994 on the second shuttle flight and, seven days after the Landsat TM image. The images were provided by the NASA JPL data putreach program, which provides radar images to researchers interested in doing studies with the data. The images in our study include two radar frequencies: an L band image at 1.24 Ghz and a C-Band image at 5.3 Ghz. For each frequency, five images are available: HH, HV, VH, VV, and total power. Only the two total power images are used in this study. The sensor is looking about 35 degrees off the nadir. Each pixel in this image represents a 12.5 by 12.5 meter square on the ground.

As in the landsat images, eight bit digital numbers represent the received intensity for each pixel. The images as received from NASA contained 8556 lines and 2620 pixels per line. This large size was awkward to work with, so a smaller image of dimensions of two thousand by three thousand pixels was extracted.

Image Registration

A. Foreshortening Error

The actual equations used to determine the geocentric position $R_t \epsilon (x,y,z)$ in SAR image formation processing are described by Curlander [11]. These three equations are:

1. Earth Model Equation. The shape of the earth is approximated by

$$\frac{x^2 + y^2}{R_e^2} + \frac{z^2}{R_p^2} = 1 \qquad (1)$$

where Re is the mean equatorial radius, $R_p = (1 - 1/f)R_e$, and f is the earth flattening factor. 2. SAR Doppler Equation. The Doppler centroid of a target is approximated by

$$f_d = \frac{2}{\lambda R_{ij}} (V_s - V_t) \cdot (R_S - R_T) \qquad (2)$$

where f_d is the doppler parameter, λ is the radar wavelength, R_{ij} is the sensor-to-target distance, or slant range, V_S is the sensor velocity, V_T is the target velocity, R_S is the sensor position, and R_T is the target position.

3. SAR range Equation. The slant range for a given pixel (i,j) is given by

$$R_{ij} = \sqrt{(R_S - R_T) \cdot (R_S - R_T)} \qquad (3)$$

These three equations are solved simultaneously using an iterative process. Note that the actual elevation of the points are not used, only a general earth model. This is the source of foreshortening error.

B. Foreshortening

Applying ground control point based image registration to the SAR-Landsat combination is difficult because of this distortion. The Shuttle Radar Lab SAR instrument transmits a pulse 1760 times per second. These pulses are separated into image rows using the doppler shift of the received pulses. The return signal received by the instrument is separated into columns by the time delay between the transmit time and the receive time. Every time delay corresponds to a distance from the sensor that the reflection must have come from. This can be viewed as an arc of equal distance from the sensor.

Although the exact point along the arc that made the reflection is unknown, the reflected signal most likely came from the point that the arc intersects the surface of the earth. To find this point, the ground is assumed to be a smooth curved surface. This means that every point on the ground in the entire image is assumed to have the same elevation. When the ground is actually smooth, this works well. However, in many places, including Northern Utah, this is not a very good assumption. For instance, our SAR image contains an elevation difference of more than 5000 feet.

The result of this poor assumption is a distortion along the rows of the image caused by differences in elevation. The lines numbered one through five in figure 1 mark five evenly spaced points. Lines 1, 2', 3', 4', and 5 mark the positions that reflections from these points would be plotted in a SAR image. Points on an uphill slope get squeezed closer together, and points on a downhill slope get stretched farther apart. This effect is known as foreshortening. This is a distortion in the image, which causes a GCP-based registration process to have an unacceptably high error.

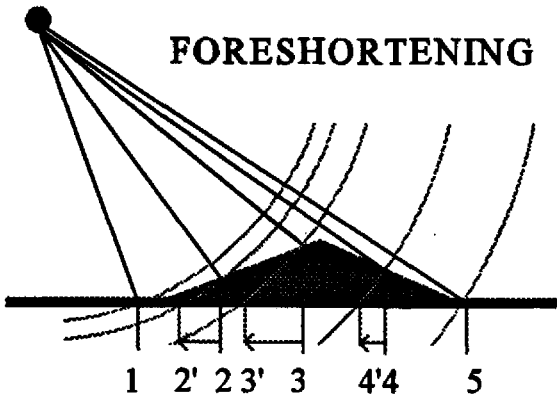

Figure 1: Radar Foreshortening

Improved Image Registration

A. Digital Elevation Model

This effect can be corrected if the elevation

of each point in the SAR image is known. Since the assumption of a smooth earth surface is no longer necessary, and the errors introduced by that assumption can be removed. To do this, an estimate of the displacement of each pixel from its proper location is computed from a Digital Elevation Model. A new SAR image is formed, using these displacement estimates to correct for the foreshortening distortion.

The DEM used was the USGS 1-degree DEM. This has data points at three arc second spacing in one degree by one degree blocks, with the same coverage as the standard USGS 1-by-2 degree quadrangle. The files were obtained by anonymous FTP from the address edcftp.cr.usgs.gov, from the directory /pub/data/DEM/250. These files are in ASCII format, with digital numbers representing the elevation in meters.[15]

The first step in creating the elevation profile of the SAR image was to download these files. They were converted into a binary format compatible with the other images in the study in order to manipulate them with the same software. Four of the 1-by-1 degree quadrangles were then mosaiced together to form a 2-by-2 degree elevation model. This covers the area from 41 to 43 degrees North latitude, and from 111 to 113 degrees West longitude.

Since the elevation is needed for every point in the SAR image and the elevation values known are in a geographic reference frame, it was necessary to find the latitude and longitude of each pixel in the SAR image. Information provided with the SAR images specified the latitude and longitude values at the corners of the image.

Using the number of pixels and the corner positions the change in latitude and longitude corresponding to a change in either line number and pixel number can be found by

$$\begin{aligned} \Delta LAT_L &= \frac{N_L LAT - N_E LAT}{L - 1}, \\ \Delta LON_L &= \frac{N_L LON - N_E LON}{L - 1}, \\ \Delta LAT_P &= \frac{F_E LAT - N_E LAT}{P - 1}, \\ \Delta LON_P &= \frac{F_E LON - N_E LON}{P - 1}. \end{aligned} \tag{4}$$

where P is the number of pixels per line, 2620 for this case, and is the number of lines in the image, 8556 for this case. The latitude and longitude of each pixel (i,j) in the SAR image S can then be calculated by adding these offsets to the known values of latitude and longitude at a corner. This is done with the equations

$$\begin{aligned} S(i,j)LAT &= N_E LAT + (i\ \Delta LAT_L) + (j\ \Delta LAT_P) \\ S(i,j)LON &= N_E LON + (i\ \Delta LON_L) + (j\ \Delta LON_P) \end{aligned} \tag{5}$$

The first point in the original DEM file is the north west corner, at 43N 113W, and there are 1200 elevation points per degree in both directions. The latitude and longitude of any point (i,j) in the original DEM file Q are simply given by

$$\begin{aligned} Q(i,j)LAT &= 43 - \frac{j}{1200} \\ Q(i,j)LON &= 113 - \frac{i}{1200} \end{aligned} \tag{6}$$

Bilinear interpolation was done to find the elevation estimate for each pixel using the four nearest DEM elevation points. This resulted in a final DEM which matched pixel for pixel with the SAR image.

B. Finding Slant Range from Platform Ephemeris

Figure 2 shows the angles and distances involved in the SAR imaging process. Relevant information includes the incidence angles, γ, at both the near and far edge of the row, and two distances: R_s, which is the distance from the center of the earth to the spacecraft, and R(1), the distance from the spacecraft to the near range ground point. Repeated use of the law of cosines allows the other needed dimensions to be calculated.

First we find R_T. This can be written in terms of R_s, R(1) and γ (1) as

$$R_T = \sqrt{R_S^2 + R(1)^2 - 2\ R_S\ R(1)\ Cos[\gamma(1)]}. \tag{7}$$

Since the ground was assumed to be smooth, R_T is constant for all pixels, we can use R_T,

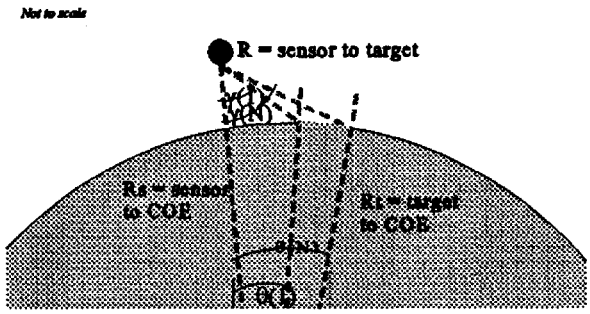

Figure 2: SAR Imaging Geometry

R_s and γ (N) can be used to find R(N), using the expression

$$R(N) = R_s\, Cos[\gamma(N)] - \sqrt{R_s^2\, Cos[\gamma(N)]^2 - R_s^2 + R_T^2}. \quad (8)$$

Using R(1) and R(N), we find the angles $\theta(1)$ and $\theta(N)$ by the expressions

$$\theta(1) = acos[\frac{R_s^2 + R_T^2 - 2\,R(1)^2}{2\,R_s\,R_T}] \quad (9)$$

and

$$\theta(N) = acos[\frac{R_s^2 + R_T^2 - 2\,R(N)^2}{2\,R_s\,R_T}]. \quad (10)$$

The assumption is then made that each pixel relates to an equal change in θ, as given by

$$\theta step = \frac{\theta(N) - \theta(1)}{N - 1}. \quad (11)$$

Given this assumption, θ at any pixel in the row can be found by expression

$$\theta(n) = \theta(1) + (n-1)\,\theta step. \quad (12)$$

Using this general formula for θ, a general expression for R can be written in terms of θ, R_s, and R_T as

$$R(n) = \sqrt{R_s^2 + R_T^2 - 2\,R_s\,R_T\,Cos[\theta(n)]}. \quad (13)$$

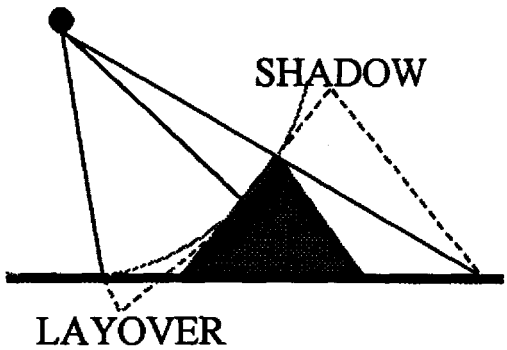

Figure 3: Radar Layover and Shadow

This is the sensor to target slant range as a function of the cross track pixel number.

C. Correcting Slant Range to Eliminate Foreshortening Error

To find the foreshortening effect, an adjusted R_T distance, $R_T'(n)$ is calculated using the value from the DEM:

$$R_T'(n) = R_T + DEM(n). \quad (14)$$

A corrected value for $\theta(n)$, $\theta'(n)$, can be expressed in terms of $R_T'(n)$ as the expression

$$\theta'(n) = acos[\frac{R_s^2 + R_T'(n)^2 - R(n)^2}{2\,R_s\,R_T'(n)}]. \quad (15)$$

This allows the shift in pixels from the correct location to be written as

$$Pixelshift(n) = \frac{\theta'(n) - \theta(n)}{\theta_{STEP}}. \quad (16)$$

A new SAR image is now formed by indexing the original image with a corrected pixel number

$$NewValue(n)=OldValue(n + Pixelshift(n)) \quad (17)$$

Since Pixelshift(n) is not an integer value, bilinear interpolation is again used to calculate the actual value used. In the case that $n + Pixelshift(n)$ is not in the range one to N, a zero value is used instead.

Radar Layover and Shadow

A. Cause

Layover and Shadow are two effects which cause invalid pixels in the SAR image. Figure 3 illustrates the cause of these effects. Layover occurs on steep uphill slopes. If the slope of the ground is steep enough that more than one point of intersection with the ground lies on the same arc of distance from the imaging platform, the reflections will be received by the radar instrument at the same time. Since the reflected power cannot be separated into the contributions of each point, the datum is unusable and no valid pixel values are available for either of these

locations. The shadow effect is caused by steep downhill slopes. If the slope of the ground is steeper than the path of the radar signal, the ground is in the shadow of the peak and no valid data are available for these locations.

B. Layover Identification

Using the DEM and sensor to image slant range, areas that are in layover can be identified. Layover areas are identified for each row independent of the others. The slant range for every point in a row is computed using equation 13. A simple test can be used to identify layover regions based on the slant range. If the sequence R(n) for a given row is strictly increasing, there will be no layover effects in that row. Every point is farther from the sensor than the one before, so there can be no overlap. However, if for any n, R(n+1) is less than or equal to R(n), there will be layover effects in that row. The range of pixels which are unknown due to the layover can be identified by finding all points for which this overlap occurs. This is illustrated in figure 4. The slant range decreases between points A and B. This causes three points on the ground to correspond to each slant range between R(A) and R(B). Since the these reflections from each of these three points cannot be distinguished, all pixel values between points C and D are invalid. The algorithm for finding this region is simply

1. Find any A points at which a decrease in R(n) begins.
2. Search forward until R(n) begins to increase. This is point B.
3. Search back from point A until R(n) is less then R(B). This is point C.
4. Search forward from point B until R(n) is greater then R(A). This is point D.
5. Mark all pixels between points C and D as invalid.

Additional precautions must be taken in forming the code to insure that more complex cases which may contain multiple peaks are correctly handled.

C. Shadow Identification

Shadow areas can also be identified using the DEM and slant range values. The first point that is in a shadow occurs when the ground drops down steeper than the path of the incoming radar signal. The drop distance, d, an be found directly from the DEM values for the pixel row, by

$$d = DEM(n) - DEM(n-1). \qquad (18)$$

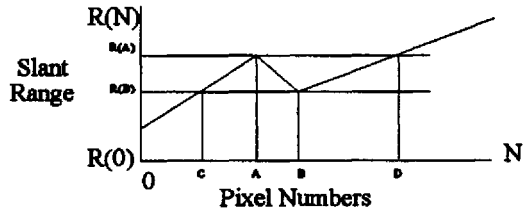

Figure 4: Layover Identification

Next, we find the angle $\alpha(n)$

$$\alpha(n) = acos\left[\frac{R(n)^2 + R_T'(n)^2 - R_S^2}{2\,R(n)\,R_T'(n)}\right] \qquad (19)$$

where R_S is the distance from the center of the earth to the spacecraft, $R_T'(N)$ is given by equation (14), and R(n) is given by equation (13). The angle of incidence of the incoming signal path, where 0 represents a nadir path, is $\eta(n)$, given by

$$\eta(n) = \pi - \alpha(n), \qquad (20)$$

where α and η are in radians. The maximum decrease in elevation which can occur without encountering shadow, h(n), is a function of $\eta(n)$

$$h(n) = \frac{w}{\tan[\eta(n)]}, \qquad (21)$$

where the w is the width of the pixel in meters, which is 12.5 meters for SIR-C images. The start of a shadow can now be identified as the lowest n value that the condition d(n) is greater than h(n) first occurs.

The shadow continues until the sum of d(n) from the start point to the end point is less than the sum of h(n) for the same range. The first point not in shadow after a region of shadow is the first point j for which the expression

$$\sum_{n=i}^{j} h(n) - \sum_{n=i}^{j} d(n) > 0 \qquad (22)$$

is true, where I is the initial point of shadow.

Results

To test whether these corrections allow a better SAR to Landsat image registration, both the original SAR image and the corrected image were registered to the Landsat image using GCPs. Erdas Imagine software on a Sun workstation was used to do the registration. Twenty GCPs were selected, and a third order fit was calculated, meaning coefficients for a polynomial with terms up to powers of three were used.

The residual error is calculated as the RMS distance between the actual location of the control points and the location they would be mapped to by this polynomial transformation function were compared. The RMS error for the original image was 9.17 pixels; for the corrected version it was 1.17 pixels.

This error term is given at the GCP locations. The error is likely to be greater at points farther from the GCPs in both cases, so this is not a measure of the maximum or average error, but the minimum error. However, it does serve as a comparison between the distorted and undistorted corrections. With this improved registration accuracy, future work can focus on applications for the combined data set.

Literature Cited

[1] Curlander, J. C., *Synthetic Aperture Radar systems and signal processing*, New York: Wiley, 1991.

[2] J. P. Pedersen, T. Guneriussen, B. Johansen, "Application of ERS-1 SAR data in combination with landsat and spot data for forestry mapping in a Norwegian forest region", in *Proc. IGARSS '93*, pp.46-48, August 1993.

[3] M. Naraghi, W. Stromberg, M. Daily, "Geometric Rectification of Radar Imagery Using Digital Elevation Models", *Photogrammetric Engineering and Remote Sensing*, Vol. 49, No. 2, pp. 195-199, February 1983.

[4] R. Kwok, J. C. Curlander, S.S. Pang, "Rectification of Terrain Induced Distortions in Radar Imagery", *Photogrammetric Engineering and Remote Sensing*, Vol. 53, No. 5, pp. 195-199, May 1987.

[5]A. J. Lewis, H. C. MacDonald, "Interpretive and Mosaicking problems of SLAR imagery", *Remote Sensing of Environment*, Vol 1, p. 231, August 1970.

[6] National Aeronautics and Space Administration, Jet Propulsion Laboratory, *SIR-C/X-SAR : earth-imaging radar for NASA's mission to planet earth.* California Institute of Technology, December 1993.

[7] M. Rast, F. Jaskolla, and K. Arnason, "Comparative digital analysis of Seasat-SAR and Landsat-TM data for Iceland", *Int. J. Remote Sensing*, Vol. 12, No. 3, pp. 527-544, March 1991.

[8] P. L. Vornberger and R. A. Bindschadler, "Multi-spectral analysis of ice sheets using co-registered SAR and TM imagery", *Int. J. Remote Sensing*, Vol. 13, No. 4, pp. 637-645, March 1992.

[9] R. Bindschalder and P Vornberger, "Interpretation of SAR Imagery of the Greenland Ice Sheet Using Coregistered TM Imagery", *Remote Sens. Environ.* Vol. 42, pp. 167-175, December 1992.

[10] J. E. Moulton and D. R. Peddle, "Assessment of the Information Content of C-Band SAR in Forest Monitoring Activities", in *Proc. IGARSS '89*, pp. 1406-1409, July 1989.

[11] J. C. Curlander, "Location of Spaceborne SAR Imagery," *IEEE Transactions on Geoscience and Remote Sensing*, Vol GE-20, No. 3, pp 359-364, July 1982.

[12] A. Fiumara and N. Pierdicca, "Evaluation of classification results obtained with combined multitemporal optical and microwave data", in *Proc. of IGARSS '89*, pp. 787-790, July 1989.

[13] S. I. A. Rahman and K. J. Dalsted, "Using SIR-A and Landsat data to study the potential of the southwestern desert of Egypt for agricultural expansion", in *Proc. of the 23rd Int. Symp. on Remote Sensing of Environment*, pp. 949-958, April 1990.

[14] B. N. Haack and E. T. Slonecker, "Merged Spaceborne Radar and Thematic Mapper Digital Data for Locating Villages in Sudan", *Photogrammetric Engineering & Remote Sensing*, Vol. 60, No. 10, pp. 1253-1257, October 1994.

[15] US Geologic Survey, National Mapping Division, *Standards for Digital Elevation Models.*US Department of the Interior, December 1992.

[16] Colwell, R. N. ed, *Manual of remote sensing.* Falls Church, Virginia: American Society of Photogrammetry, 1983.

[17] National Aeronautics and Space Administration, Scientific and Technical Information Branch, *Synthetic aperture radar/Landsat MSS image registration.* Springfield, Virginia: National Technical Information Service, 1979.